Nonlinear Guidance for a Transfer Orbit to the Moon

Andrea Sesta[(1)], Daniele Durante[(2)], Luciano Iess[(3)], Lorenzo Bucci[(4)], Ruaraidh Mackenzie[(5)]

[(1)] Department of Mechanical and Aerospace Engineering, University of Rome La Sapienza
Rome, Italy
Email: andrea.sesta@uniroma1.it

[(2)] Department of Mechanical and Aerospace Engineering, University of Rome La Sapienza
Rome, Italy
Email: daniele.durante@uniroma1.it

[(3)] Department of Mechanical and Aerospace Engineering, University of Rome La Sapienza
Rome, Italy
Email: luciano.iess@uniroma1.it

[(4)] DEIMOS Space for ESA - European Space Agency
Darmstadt, Germany
Email: lorenzo.bucci@ext.esa.int

[(5)] OPS-GFA at ESA/ESOC
Darmstadt, Germany
Email: ruaraidh.mackenzie@esa.int

***Abstract* – The purpose of this work is to present a nonlinear guidance algorithm for spacecraft navigation that can be applied in any mission scenario. This approach allows to reliably estimate the navigation Delta-V (ΔV) budget and obtain a more accurate and reliable orbit insertion performance.**

The proposed nonlinear guidance algorithm is applied for a lunar mission scenario, focusing on the transfer orbit up to lunar orbit injection. The key performance parameters under analysis include the navigation ΔV budget for the mission and the orbital parameters scattering at arrival with respect to the targets. To perform a realistic and reliable analysis, the study takes into account the main factors that affect spacecraft navigation, namely the accuracy of the launcher insertion, the manoeuvres execution errors, and the knowledge of the spacecraft state. As a last step, we investigate how the navigation performances are affected by the ground station operations schedule, namely by the orbit determination arc and the flight dynamics operations cycle. The duration of the orbit determination arc is related to the observation time window used to estimate the spacecraft's position. The flight dynamics operations cycle consists of the timing for the ground infrastructure procedures, such as orbit determination, manoeuvres planning, and TT&C.

I. INTRODUCTION

In recent years, the Moon has drawn significant attention not only from space agencies (such as NASA [1],ESA [2], JAXA [3] and ISRO [4]) but also from private entities. Numerous commercials and institutional missions are already planned for the upcoming decade [5]. This renewed focus on the Moon comes from several factors, including the desire to establish a permanent human presence on our satellite, its potential as a testing ground for crucial technologies needed for deep space exploration (particularly for future manned missions to Mars), and the recent discovery of water ice at the Moon's South Pole [6].

Even if each mission has different goals, all of them share the same necessity for guidance and navigation, with different constraints. A usual approach for deep-space mission design is to adopt linear guidance for the spacecraft. However, in a lunar transfer scenario due to its high non-linearity especially in the lunar orbit insertion phase, this approximation can lead to inaccurate orbit targeting and underestimation of the navigation Delta-V (ΔV) budget, together with large and unrealistic dispersions. The navigation ΔV budget is defined as the difference between the design ΔV and the required ΔV not only to reach the reference orbit but also to compensate for the mission perturbations inside a certain confidence interval. The orbit insertion performance is evaluated as the scatter of the final orbit parameters with respect to the design ones.

This paper aims to present a nonlinear navigation algorithm for lunar transfer trajectories. While the associated numerical simulations are tailored to a specific scenario, the methodology outlined can be applied to various mission definitions. Estimating the navigation ΔV budget of the proposed algorithm is essential.

The proposed nonlinear navigation algorithm allows us to improve not only the targeting performance but also

the propellant consumption, especially for a highly nonlinear problem, such as in the analysed lunar transfer orbit.

The research considers that both the orbit determination and the navigation of the satellite are performed at the ground station, hence the computational burden is not reflected on the spacecraft design. The major drawback of the nonlinear guidance with respect to the approximated linear one is the increased computational cost of the procedure.

The simulation was performed with the ESA/ESOC flight dynamics software GODOT (General Orbit Determination and Optimization Toolkit), which allows users to perform orbit-related computations for estimation, optimization, and analysis of orbits for mission analysis and in-flight operations [7]. For the navigation analysis, the GODOT software was used in conjunction with PyGMO, a scientific library providing many parallelizable optimisation problems and algorithms [8].

The paper structure is the following:

- Section II presents the simulation setup, namely the orbit geometry, the Orbit Determination (OD) assumptions, and the navigation algorithm.
- Section III sums up the results for a conservative scenario of the lunar transfer orbit.
- Section IV shows the difference in performance of the guidance algorithm changing the navigation assumptions.
- Section V summarizes the results and performances of the proposed approach.

II. Simulation Setup

The nonlinear guidance algorithm is tested on a lunar transfer scenario, targeting a low lunar circular polar orbit with radius equal to 1838.1 km, thus an altitude of 100.7 km using the Moon mean radius of 1737.4 km. The selected target orbit is particularly relevant and suitable for the Moon exploration and observation (see [9], [10] and [11]).

A. Lunar Transfer Geometry

The navigation analysis examines various design trajectories spanning five years to assess the impact of the Earth-Moon relative geometry on the lunar transfer orbit and guidance performance. The design trajectories were optimized to perform the lunar transfer targeting the Moon at the ascending or descending node, minimizing the propellant consumption [11]. This stems from the assumption of launching from Kourou with a maximum performance, low-inclination lunar transfer orbit. The schema for the lunar transfer trajectory includes:

- Launcher separation (SEP).
- Apogee Correction Manoeuvre (ACM), 1 day after launcher separation. It can be adjusted, see section III.
- Trajectory Correction Manoeuvre (TCM) if necessary. It is executed at least 1 day after the ACM and 1 day before the Lunar Orbit Insertion (LOI). It can be adjusted, see section III.
- Lunar orbit insertion.

The Time Of Flight (TOF) for the transfer orbit depends on the specific solution, according to the launch day within a launch period. However, the spacecraft always performs only one ACM and TCM during the lunar transfer. Additionally, each launch opportunity presents multiple possible trajectories within a specific launch window. This analysis does not address the design of the lunar transfer orbit itself (done in [11]); it focuses on evaluating the satellite guidance performance along a predetermined trajectory.

Fig. 1 illustrates the different lunar transfer orbits for a selected launch window among those analysed over five years.

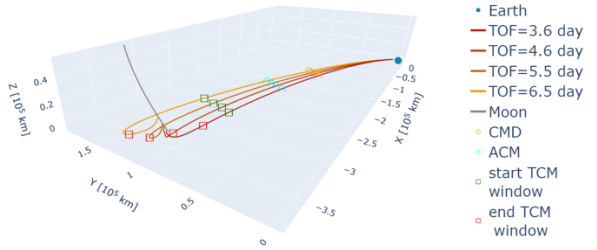

Fig. 1. A typical set of lunar transfer orbit 3-dimensional representation in the EMEJ2000 reference frame for a selected launch window.

B. Orbit Determination Assumptions

The primary goal of orbit determination is to ascertain the dynamic state of a spacecraft, specifically its position and velocity evolution over time. This process relies on precise measurements of observable quantities and accurate models describing spacecraft dynamics and observables [12].

The numerical simulation of the OD process involves two main stages: data simulation and parameter estimation. During the data simulation phase, reference trajectories (considered the "real" or "true" trajectories) are generated, along with corresponding observed observables. In the subsequent estimation phase, these simulated data along with computed observables derived from observation equations, undergo processing. A batch least-squares filter is employed to refine first-guess trajectories and adjust other parameters within the dynamical model.

The orbit determination of the spacecraft during the lunar transfer orbit is assumed to be performed on the ground. The satellite establishes a two-way coherent radio link in the X-band with the stations of the European Space Tracking Network (ESTRACK), namely Cebreros (Spain), New Norcia (Australia), and Malargüe (Argentina). Therefore, in the orbit

determination, two-way range and Doppler observables are processed. Table 1 presents conservative assumptions regarding the measurement noise and sampling time for a typical mission, given that we did not perform a detailed error budget for the radio link between the spacecraft and the stations.

Table 1. Measurement noise and count time for the radio-tracking observables.

Observations	Noise	Count Time
Range	2 m	1 hour
Doppler	0.3 mm/s	60 s

In any OD process, inaccuracies within the dynamical model arising from missing or poorly modelled accelerations inevitably introduce biases in the estimated model parameters [13]. For instance, accurately modelling the Solar Radiation Pressure (SRP) acceleration acting on the spacecraft proves challenging, with errors often exceeding 2% of the central value [14]. In the estimation phase, we accounted for these inaccuracies by incorporating estimated stochastic accelerations into the dynamical model. This adjustment addresses potential discrepancies in a realistic scenario due to dynamical mismodeling. While various formulations could be utilized for this purpose, we opted for a stochastic piecewise-constant accelerations model for this analysis with an apriori uncertainty of the order of 10^{-10} m/s^2 on each component in the International Celestial Reference Frame (ICRF). The other estimated parameters in the OD filter are:

- spacecraft dynamical state at the launcher separation epoch defined as Keplerian parameters with an apriori uncertainty vector of 1 km for the pericentre and apocenter radius and 6° for inclination, RAAN, the argument of perigee and true anomaly.
- range biases for each tracking station with an apriori uncertainty of 10 m.
- manoeuvre with an apriori uncertainty of 1 m/s.

C. Nonlinear guidance algorithm

The proposed nonlinear guidance algorithm, depicted in Fig. 2, is applied to the reference lunar transfer orbit. However, the same approach is suitable for any satellite orbit and scenario.

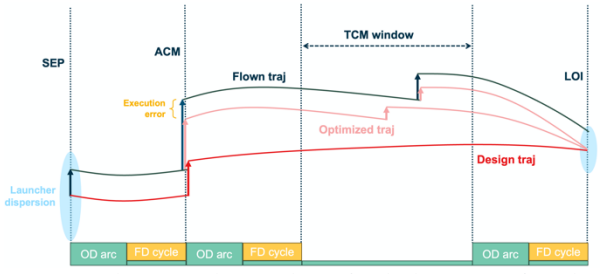

Fig. 2. Nonlinear guidance scheme for the lunar transfer orbit.

As depicted in Fig. 2, the process begins with an orbit determination arc followed by a command point. At this point, the estimated trajectory is used to optimize the following manoeuvres to minimize the propellant consumption and reach the desired target orbit. When determining the design manoeuvres, it is crucial to consider the Flight Dynamic (FD) cycle, which dictates constraints on the earliest epoch for manoeuvre execution. The FD cycle encompasses all operations required for spacecraft navigation, from orbit determination to telecommand uploads for manoeuvre execution.

To estimate the navigation budget and the targeting accuracy of the desired orbit, we conducted a Monte Carlo analysis on a set of designed trajectories spanning a 5-year period. We perturbed the initial satellite state of each trajectory according to a putative launcher dispersion to generate 1000 sample reference trajectories with a standard deviation of 2 km in position and 1 m/s in velocity for each 3D component. We then apply the navigation algorithm presented in Fig. 2 to each sample. It involves propagating the initial perturbed state to the command point and performing the OD process with the collected observations to obtain the estimated trajectory and the associated covariance matrix (to compute the uncertainty evolution over time on position and velocity). The estimated covariance matrix is used to perturb the trajectory to introduce the error related to the spacecraft positioning accuracy. This OD perturbed trajectory is the one used for the optimization procedure to design the commanded manoeuvre to reach the target orbit while minimizing the propellant consumption.

After this, to emulate a realistic scenario, we apply a Gaussian manoeuvre execution error on both the magnitude and the thrusting direction with a standard deviation of 1% in the ΔV magnitude and 1° in the pointing direction to reflect a realistic propulsion system and obtain the executed manoeuvre. Finally, the executed manoeuvre is applied to the reference sample obtaining the trajectory flown by the spacecraft.

The same procedure is applied for each couple of command point-manoeuvre with the constrain that the time interval between the command point and the previous manoeuvre is the OD arc duration, while the time span between the command point and the next manoeuvre is at least the duration of the FD cycle.

In this paper, for computational efficiency, we perform the orbit determination process only for the design trajectory and use the same covariance matrix evolution for all the Monte Carlo samples. This is an acceptable assumption given that the initial perturbation related to the launcher dispersion does not significantly modify the covariance matrix evolution of the new reference lunar transfer orbit with respect to the design one.

The duration of the OD arc and FD cycle impact the manoeuvre execution epochs, thus the associated navigation budget for the lunar transfer orbit. Moreover, the number of observables collected during the OD arc affects the orbit reconstruction accuracy and, therefore, the covariance matrix evolution, especially at the control point.

This analysis focuses on the orbit targeting and navigation budget just before the LOI, given that the lunar orbit insertion procedure can be further optimized by considering different approaches, also according to the orbital parameters scattered at the end of the lunar transfer trajectory.

III. Simulation Results

In this study, we explored various scenarios by adjusting the durations of the orbit determination arc and flight dynamics cycle to investigate their impact on the navigation budget for the lunar transfer orbit, as represented in Table 2.

Table 2. OD arc and FD cycle durations for the analysed scenarios.

Case	OD arc	FD cycle
Conservative	12 h	12 h
Mean	8 h	8 h
Best	8 h	4 h

A. Monte Carlo analysis for a single design trajectory

The reference scenario, and the more conservative one, assumes OD arc and FD cycle durations of 12 hours each, requiring the ACM to be executed at least a day after launcher separation. Fig. 3 and Fig. 4 depict the position and velocity accuracy over time for one of the analysed design trajectories. Despite differences in reference epoch and time of flight for each lunar transfer orbit, the covariance evolution of the satellite state exhibits a similar trend. It is important to stress that both Fig. 3 and Fig. 4 show the uncertainty of the desired state component at various epochs, processing only the observations before each epoch.

The discrepancy in accuracy between the x and y components of position and velocity, compared to others (almost one order of magnitude), can be attributed to orbit geometry. In fact, the lunar transfer orbital plane nearly aligns with the Earth's equatorial plane (close to the X-Y ICRF plane), resulting in radio tracking data collected predominantly along these two directions. The spike in the velocity components uncertainty represented in Fig. 4 is associated with the ACM execution in the design trajectory.

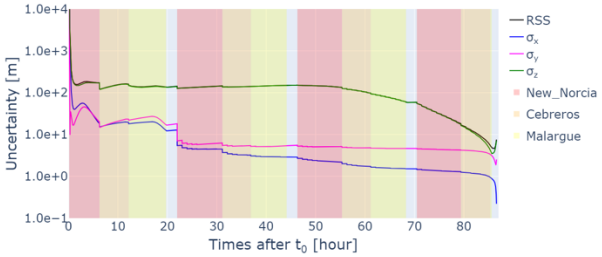

Fig. 3. Satellite position uncertainty components and their root sum of squares (RSS) in ICRF as a function of the time after launcher separation. The blue, magenta, green, and black curves represent, respectively, the X, Y, and Z components and the norm of the position uncertainty. The shaded area represents the timeslots of tracking data for each ground station, namely New Norcia (red), Cebreros (orange), and Malargüe (yellow).

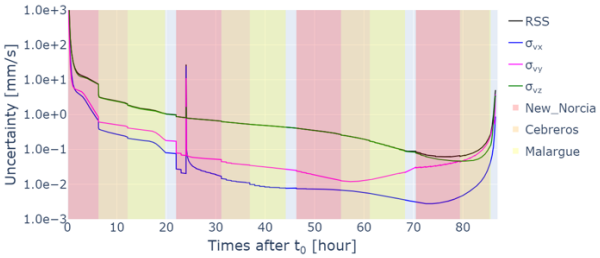

Fig. 4. Satellite velocity uncertainty components and their RSS in ICRF as a function of the time after launcher separation. The blue, magenta, green, and black curves represent, respectively, the X, Y, and Z components and the norm of the velocity uncertainty. The shaded area represents the timeslots of tracking data for each ground station, namely New Norcia (red), Cebreros (orange), and Malargüe (yellow).

Fig. 5 depicts the range of the executed (commanded plus execution error) ACMs and TCMs across all the perturbed reference trajectories (1000 samples) compared to the values of the design trajectory. These values are a function of the relative change in specific orbital energy (ΔE) between each perturbed trajectory and the design trajectory at launcher separation.

The ACMs are optimized to compensate for the launcher dispersion at separation, as their evolution shows a strong correlation with the change in orbital energy. The scattering of ACMs around this trend is related to the manoeuvre execution error. Meanwhile, the TCMs mainly recover the ACM execution error and the orbit determination error at the first command point.

Fig. 5 highlights that some reference trajectories exhibit a lower executed manoeuvre ΔV than the design trajectory, leading to reduced propellant consumption and a higher spacecraft mass at lunar insertion. This difference arises because launcher dispersion modifies the satellite's state in such a way that part of the required ACM ΔV is provided by the launcher. However, these more efficient lunar transfer orbits were not identified during trajectory design because the launcher needs to exceed its nominal performance to obtain them. For example, it can insert the same spacecraft mass on a higher energy orbit.

For each design orbit, the relation between the ACM and the ΔE changes due to the Earth-Moon relative geometry. The general trend is a parabola where the ACM is minimized for a certain orbit energy. If the launcher inserts the spacecraft on a more (or less) energetic orbit, the ACM must compensate for this additional (or decreased) energy. However, achieving these optimal trajectories with nominal launcher performances is not always feasible.

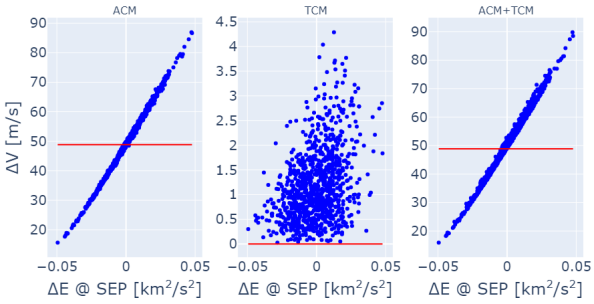

Fig. 5. Executed ACM (left), TCM (middle), and their sum (right) as a function of the change in specific orbital energy between each perturbed reference trajectory (1000 samples) and the design orbit at launcher separation. The horizontal red line represents the design value for the respective manoeuvre.

Finally, Fig. 6 shows the orbital parameters scattering before the lunar orbit insertion as a function of the sample number. It represents the targeting accuracy of the proposed nonlinear guidance algorithm. It is important to note that the parameter scattering is mainly related to the TCM execution error and the orbit determination accuracy at the associated command point. Indeed, the optimized trajectory correction manoeuvre is designed to target the desired spacecraft state.

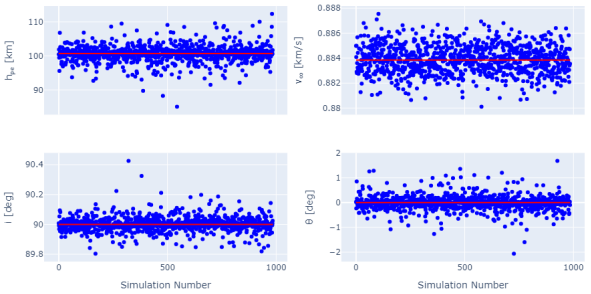

Fig. 6. Orbital parameters scattering before the LOI as a function of the sample number. From left to right, the first row shows the pericentre altitude and the hyperbolic excess velocity. The second row represents the inclination and the true anomaly. The horizontal red line in each plot indicates the desired target values.

B. Lunar transfer performance

We conducted the same Monte Carlo analysis for all design trajectories, assuming an OD arc and FD cycle duration of 12 hours.

Due to the significant nonlinearity of the problem under consideration, the distribution of orbital parameters before the LOI with respect to the design values is not symmetric. Therefore, we computed a pseudo 3-σ standard deviation of the resulting distribution for each individual case to observe trends over the analysed time span. This value is calculated by determining the difference between the 99.85th and 0.15th percentile values (thus encompassing 99.7% of the samples) of the distribution of interest and then dividing it by 2. This formulation allows us to account for both the overshooting and undershooting cases, thereby avoiding potential overestimation of targeting performance.

Fig. 7 depicts the pseudo 3-σ scatter for the pericentre altitude, inclination, and true anomaly of the various design trajectories as a function of the launcher separation epoch. In most cases, it is possible to target the desired low lunar circular polar orbit with an accuracy of approximately 10 km in altitude, 0.3° in inclination, and 1.0° in true anomaly.

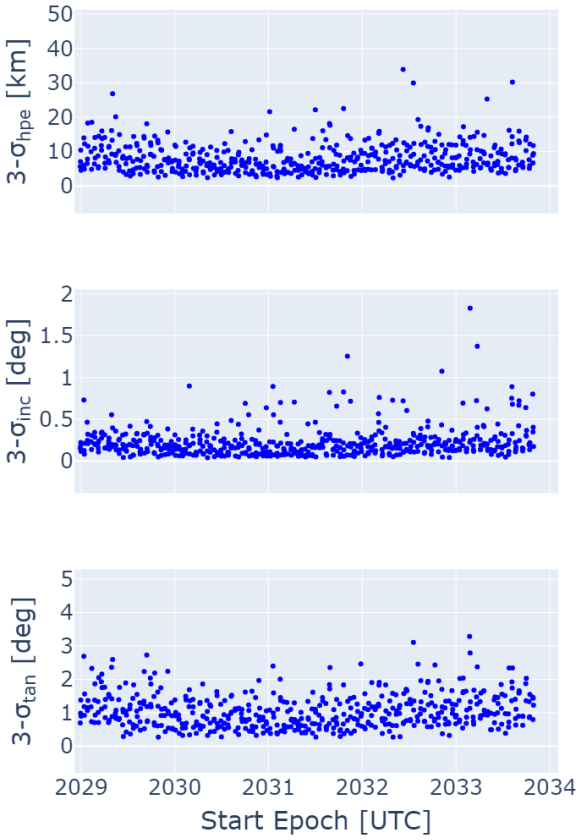

Fig. 7. Orbital parameters (before LOI) pseudo 3-σ as a function of the launcher separation epoch, namely pericentre altitude (top), inclination (middle) and true anomaly (bottom).

Instead Fig. 8 represents the 99.7th percentile of the hyperbolic excess velocity for the different launcher separation epochs. In this last case, we adopt the 99.7th percentile because we are interested in the actual values of the overshooting side of the distribution (higher energy than the design trajectory) rather than the accuracy with respect to the target variable. Indeed, given that the hyperbolic excess velocity represents the specific orbital energy of the lunar transfer orbit, and that the energy of the target low circular orbit is known given the semi-major axis, Fig. 8 represents the orbital energy variation needed for the lunar orbit insertion procedure.

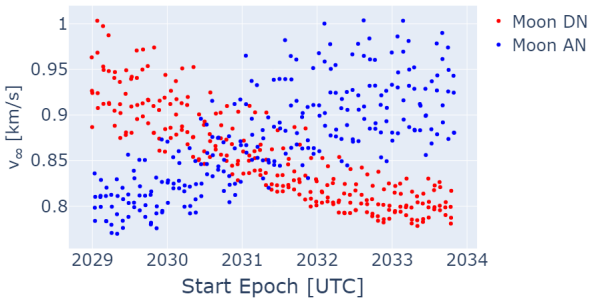

Fig. 8. Hyperbolic excess velocity 99.97th percentile as a function of the launcher separation epoch.

The navigation budget for the analysed lunar transfer orbit is about 35 m/s, as shown in Fig. 9. It represents the 99.7th percentile of the difference between the executed manoeuvres (commanded plus execution error) and the design ones for each launcher separation epoch.

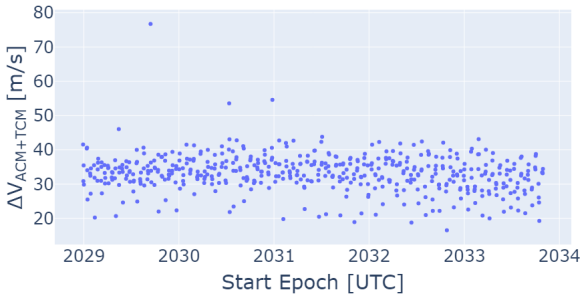

Fig. 9. Navigation budget defined as the difference between the 99.7th percentile of the executed manoeuvres and the design ones as a function of the launcher separation epoch.

IV. Supplementary Analysis

This paper analyses the effect of different assumptions on the OD arc and FD cycle durations, see Table 2. As said before, decreasing the OD arc duration allows us to decrease the time between the manoeuvre and the successive command point, but at the same time, it reduces the number of observables collected, therefore, the positioning accuracy of the satellite. On one hand, decreasing the OD arc duration allows to anticipate the manoeuvre, especially the ACM after launcher separation, thus reducing the requested ΔV (lower gravitational losses). On the other hand, the reduced number of observables affects the satellite orbit reconstruction decreasing the positioning accuracy, thus increasing the perturbation on the trajectory used to optimize the commanded manoeuvres that are going to affect the propellant consumption of the successive manoeuvres.

The reduction of the FD cycle decreases the minimum required time between the control point and the successive manoeuvre. This reduction allows us to anticipate the manoeuvre and reduce the propellant consumption as the OD arc without the drawback of the reduced positioning accuracy. However, it is not possible to freely decrease the FD cycle duration given that it is related to a series of necessary operations at the ground station to allow satellite navigation (such as the OD process or the telecommand generation and uploading).

Fig. 10 represents the propellant consumption comparison between the conservative case analysed in the previous subsection (OD arc and FD cycle of 12 hours) and a mean and best-case scenario, with an OD arc of 8 hours for both and an FD cycle duration of 8 hours and 4 hours respectively. The comparison is on a subset of the previously analysed trajectories, and it shows that the average propellant consumption with respect to the conservative approach decreases by ~11 m/s for the mean-case scenario and ~17 m/s for the best-case one.

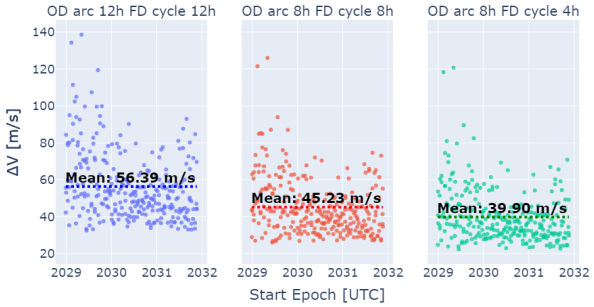

Fig. 10. Executed manoeuvres ΔV as a function of the launcher separation epoch. The blue, red, and green scatter points represent, respectively, the conservative (left), mean (middle), and best-case (right) scenarios. The corresponding dotted lines represent the average values.

V. Conclusion

This paper introduces a nonlinear guidance algorithm designed for spacecraft navigation across various mission scenarios. In this study, we apply the algorithm to analyse a lunar transfer orbit, focusing on evaluating both targeting accuracy and the associated navigation budget. We operate under the assumption that the ground station will execute the procedure.

In the conservative scenario discussed earlier, the guidance algorithm, accounting for a presumed manoeuvre execution error (1% in magnitude and 1° in thrusting direction), ensures precise targeting to the desired low lunar polar circular orbit. Specifically, it achieves an accuracy of approximately 10 km in pericentre altitude and 0.3° in inclination. The navigation budget estimated for this scenario is around ~35 m/s.

Additionally, this analysis considers the impact of varying the duration of the orbit determination arc and the flight dynamics cycle on propellant consumption. Reducing both time intervals decreases the required ΔV for the lunar transfer orbit, in the best-case scenario of ~17 m/s. However, practical constraints limit the extent to which these time intervals can be reduced. For instance, decreasing the OD arc reduces the number of radio-tracking data collected, thus affecting satellite

state reconstruction and accuracy. Similarly, constraints on the FD cycle derive from essential ground operations such as the OD process and telecommand generation and upload.

Nevertheless, one potential solution is to implement the same navigation algorithm onboard the satellite, allowing for autonomous guidance. This approach significantly shortens the FD cycle to only the computational time needed for applying the nonlinear guidance scheme onboard the spacecraft. In conjunction with this onboard navigation approach, it is possible to utilize a space-born GNSS receiver [15] to perform the OD process autonomously. Moreover, using GNSS pseudo-range and pseudo-range rate observables allows us to obtain an accurate positioning, especially right after the launcher separation which happens below the GNSS satellite orbits. Finally, this onboard autonomous guidance approach reduces the time interval between each manoeuvre, thus allowing to perform more manoeuvres during the lunar transfer orbit.

VI. References

[1] National Aeronautics and Space Administration (NASA), "Artemis." Accessed: Mar. 20, 2024. [Online]. Available: https://www.nasa.gov/feature/artemis/

[2] European Space Agency (ESA), "Argonaut." Accessed: Mar. 20, 2024. [Online]. Available: https://www.esa.int/Science_Exploration/Human_and_Robotic_Exploration/Exploration/Argonaut

[3] T. Hoshino *et al.*, "Lunar polar exploration mission for water prospection - JAXA's current status of joint study with ISRO," *Acta Astronaut*, vol. 176, pp. 52–58, Nov. 2020, doi: 10.1016/j.actaastro.2020.05.054.

[4] S. Biswas and S. Biswas, "Chandrayaan 3 and Other Moon Missions: An Update and Review," *SSRN Electronic Journal*, 2023, doi: 10.2139/ssrn.4553155.

[5] National Aeronautics and Space Administration (NASA), "NASA names companies to develop human landers for Artemis moon missions." Accessed: Mar. 20, 2024. [Online]. Available: https://www.nasa.gov/news-release/nasa-names-companies-to-develop-human-landers-for-artemis-moon-missions/

[6] International Space Exploration Coordination Group, "The Global Exploration Roadmap," 2018. [Online]. Available: www.globalspaceexploration.org.

[7] European Space Agency (ESA), "GODOT Documentation." Accessed: Apr. 04, 2024. [Online]. Available: https://godot.io.esa.int/godotpy

[8] F. Biscani and D. Izzo, "A parallel global multiobjective framework for optimization: pagmo," *J Open Source Softw*, vol. 5, no. 53, p. 2338, Sep. 2020, doi: 10.21105/joss.02338.

[9] B. L. Ehlmann *et al.*, "NASA's Lunar Trailblazer Mission: A Pioneering Small Satellite for Lunar Water and Lunar Geology," in *2022 IEEE Aerospace Conference (AERO)*, 2022, pp. 1–14. doi: 10.1109/AERO53065.2022.9843663.

[10] N. Baresi *et al.*, *Mission Analysis and Design of VMMO: The Volatile Mineralogy Mapping Orbiter*. 2021.

[11] L. Bucci, F. Renk, and W. Martens, "Argonaut Mission Analysis Guidelines, ESA-E3P-EL3-TN-005, Issue 1, Revision 8," 2023.

[12] B. D. Tapley, G. H. Born, and B. E. Schutz, *Statistical Orbit Determination*. Elsevier, 2004. doi: 10.1016/B978-0-12-683630-1.X5019-X.

[13] G. Bury, K. Sośnica, R. Zajdel, and D. Strugarek, "Toward the 1-cm Galileo orbits: challenges in modeling of perturbing forces," *J Geod*, vol. 94, no. 2, p. 16, Feb. 2020, doi: 10.1007/s00190-020-01342-2.

[14] R. S. Park, S. W. Asmar, E. G. Fahnestock, A. S. Konopliv, W. Lu, and M. M. Watkins, "Gravity Recovery and Interior Laboratory Simulations of Static and Temporal Gravity Field," *J Spacecr Rockets*, vol. 49, no. 2, pp. 390–400, Mar. 2012, doi: 10.2514/1.A32117.

[15] V. Capuano *et al.*, "Standalone GPS L1 C/A Receiver for Lunar Missions," *Sensors*, vol. 16, no. 3, p. 347, Mar. 2016, doi: 10.3390/s16030347.